scientific reports

Check for updates

OPEN

Active infrared tuning of metal–insulator-metal resonances by VO_2 thin film

Emilija Petronijevic[1], Maria Cristina Larciprete[1]✉, Marco Centini[1], Lucilla Pronti[2], Vincenzo Aglieri[3,4,5], Luca Razzari[5], Andrea Toma[4], Roberto Macaluso[3], Roberto Li Voti[1] & Concita Sibilia[1]

VO_2 is a promising phase change material offering a large contrast of electric, thermal, and optical properties when transitioning from semiconductor to metallic phase. Here we show that a hybrid metamaterial obtained by proper combination of a VO_2 layer and a nanodisk gold array provides a tunable plasmonic gap resonance in the infrared range. Specifically, we have designed and fabricated a metal–insulator-metal gap resonance by inserting sub-wavelength VO_2 film between a flat gold layer and a gold nanodisk resonator array. The resonance of the hybrid metamaterial is centered in the useful 3–5 μm range when VO_2 is in its semiconductor state. The experimental study highlights a monotonical spectral tuning of the resonance when increasing temperature up to 50 °C above the room temperature, providing a continuous resonance shift of almost 1 μm in the mid-infrared range. Wavelength range and intensity tunability can be further optimized by modifying the thicknesses of the layers and metamaterial parameters.

Keywords Plasmonics, Phase change materials, Metamaterials, VO_2

Vanadium dioxide (VO_2) is a phase change material (PCM) that exhibits a sharp structural lattice change from a monoclinic phase, characterized by a semiconducting state, to a tetragonal (rutile) phase, exhibiting metallic behavior. This phase change occurs at a relatively low transition temperature (T_C), i.e. around 68 °C[1–4]. Furthermore, by doping vanadium dioxide, for example with tungsten, it is possible to tune the phase transition temperature, bringing it to values close to room temperature[5,6]. During the semiconductor-to-metal phase transition (SMT) and back, the dispersion law of the complex refractive index n + ik gets strongly modified, leading to abrupt changes of the optical properties[7–10]. Being a very efficient thermochromic material, VO_2 has been extensively studied in the seek for active control of thermal emission, attracting interest in applications in infrared optical systems, smart windows, "smart" blackbody devices for spacecraft, light modulators, and photonic crystals[11–17]. Thermally induced SMT in VO_2 can be nowadays obtained with nanoscale heaters[18], while the optically induced SMT allows for femtosecond timescale[19], opening new potentialities in ultrafast optical switching[20,21].

As micro/nanotechnology advances, tuneable properties of VO_2 are being used in combination with nanostructured media, thus allowing for numerous degrees of freedom in electromagnetic manipulation. An asymmetric Fabry–Perot (FP) cavity based on an ultra-thin VO_2 was discovered to lead to almost perfect SMT switching of absorption at 11.75 μm[22], while its combination with Au microresonators led to both FP and metamaterial infrared resonances[23]. Different metamaterial geometries combined with VO_2 have been explored since: split ring resonators,[24,25] periodic gratings and cylinders,[26] Al circular patch arrays,[27] sub 10-nm gap metamaterials resonating in the near-infrared[28] etc. Furthermore, patterning of VO_2 into metasurfaces has enabled smart thermal emitters for thermal management, which is of great importance for both terrestrial and space radiative cooling applications[29,30]. Metal–insulator-metal (MIM) designs were proposed for multiple resonance tuning in the near-infrared range[31], and for tunable emission of magnetic dipolar emitters at 1.54 μm[32].

In a more complex configuration[33], we designed a plasmonic metamaterial hybridized with VO_2, with the optimized resonant absorption behavior in the 3–5 μm, i.e. Mid-wave infrared range (MWIR) range. Specifically, the investigated metamaterial design consists of a thin layer of VO_2 sandwiched between an Au ground layer and

[1]Department SBAI, Sapienza University of Roma, Via A. Scarpa 14, 00161 Rome, Italy. [2]National Laboratories of Frascati - INFN, Via Enrico Fermi 54, 00044 Frascati, Rome, Italy. [3]Department of Engineering, University of Palermo, Viale delle Scienze, 90128 Palermo, Italy. [4]Clean Room Facility, Istituto Italiano di Tecnologia, Via Morego 30, 16163 Genova, Italy. [5]Institut National de la Recherche Scientifique – Énergie Matériaux et Télécommunications, 1650 Boulevard Lionel-Boulet, Varennes, QC J3X 1P7, Canada. ✉email: mariacristina.larciprete@uniroma1.it

the Au nanodisks metamaterial. This structure displays MIM resonance when VO_2 is in its semiconductor, i.e. cold state. The resonant behavior disappears when the VO_2 layer is heated to the transition temperature: metallic VO_2 becomes reflective as the underlying Au layer. Several factors such as disk dimensions and periodicity can be adjusted in order to achieve almost unitary absorption in the desired spectral range, which can be switched to zero absorption by changing the VO_2 phase. Such behavior can be applied in thermal camouflage systems[34,35], thus the need for the experimental confirmation of our numerical proposal.

Pulsed laser deposition (PLD) is a very versatile and low-cost deposition technique which has been widely used to produce high quality VO_2 thin films without the need for a post-growth annealing step[36,37]. Beside deposition parameters such as temperature and oxygen pressure, VO_2 films optical properties depend also on films thickness. In particular, optical properties such as IR emissivity, show a dynamic range dependent on the films thickness due to a correlation with the crystalline grain size.[37].

Following the numerical study and inspired by our previous experimental results,[4,5] we here experimentally investigate a structure composed by a thin VO_2 layer, deposited by PLD, with a specially designed metamaterial. The present design is based on the tunable resonant absorption achievable in the MIM switchable structure. We experimentally demonstrate a monotonical tuning of the absorption intensity and resonance in the 3–5 μm range as a function of temperature. Finally, we employ detailed numerical modelling to highlight how resonances are affected by the phase transition and how they depend on the fraction of the transitioned part of VO_2.

Results and discussion

Sample design

Our sample is based on the resonant absorption in the MIM type of the designs[38,39]. The metamaterial design consists of a thin layer of VO_2 inserted between a 2D matrix of gold nanodisks and a thin continuous gold film, as schematically depicted in the Fig. 1a; the whole metamaterial sits on a CaF_2 substrate. This structure provides a typical MIM resonance when VO_2 layer is in its semiconductor state (i.e., at room temperature). Several parameters such as metamaterial periodicity p, nanodisk radius r, nanodisk height h, VO_2 film and Au ground layer thicknesses, can be optimized to get tuning of the MIM resonance position within the range of interest. When the VO_2 layer is heated above the transition temperature, it turns into a metallic state thus it becomes reflective, as the underlying Au layer. Therefore, we can expect a resulting increase of the reflectivity with respect to the resonant state. Moreover, at intermediate temperatures where VO_2 has not completely transitioned, it will be possible to exploit a continuous spectral tuning of the resonance, as we show in the following paragraph in the experimental section.

For what concerns the Au metamaterial design, the absorption contrast due to SMT in the infrared range was investigated using full-wave 3D electromagnetic simulations based on finite difference time domain (FDTD) commercially available solver by Lumerical[40]. The details of the simulation procedure are given in *Methods*; the optimization of the MWIR contrast was done in the parameter space of the design geometry[30,31,41] The fabrication details are given in *Methods*, while Fig. 1b shows a representative micrograph of the fabricated device.

Experimental and numerical investigation

Spectral IR reflectivity (R) measurements of the VO_2/Au based metamaterial were performed using a Bruker VERTEX 70v FTIR spectrometer coupled with the Hyperion microscope at the INFN-LNF Dafne-Light facility in Frascati. The IR source was a globar while the detector was a liquid nitrogen-cooled mercury – cadmium – telluride photovoltaic element. Concerning with measurement reproducibility, for each measurement a total number of 64 interferograms were acquired, with a spectral resolution of 4 cm^{-1}. The spectral averaging of obtained scans was applied when calculating the reflectivity to improve the signal-to-noise ratio. The sample was placed onto a stabilized heat source (Linkam THMS600 Heating and Freezing stage system) and a control thermocouple was placed in contact with the sample surface to monitor the actual temperature evolution of the sample during measurements. Spectra were collected at different temperatures, ranging from room temperature (26 °C) to 100 °C. Finally, the obtained measurement data were normalized to the spectra of a gold reference mirror. The absorption was calculated as 1-R.

In Fig. 2a, we show the different spectra of the VO_2-based hybrid metamaterial obtained when it is heated from room temperature to 100 °C. Experimental results show that there is an efficient tuning of the resonance with increasing temperature. First evidence from Fig. 2a is a large dip in reflectance for the room-temperature (RT) curve at 4.72 μm, which corresponds to the plasmonic gap resonance due to the Au nanodisks metamaterial. This mode is red-shifted as the temperature increases due to the modified dielectric constant of the VO_2 layer

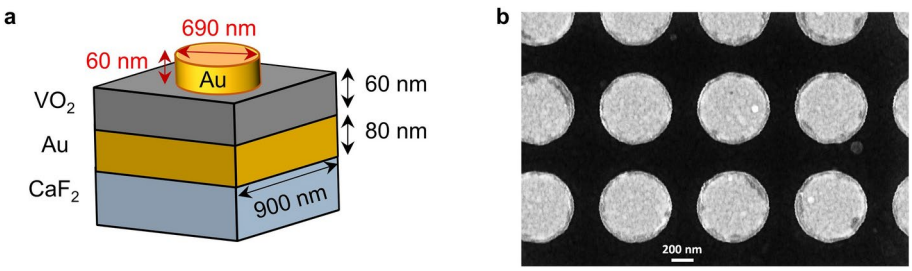

Fig. 1. (**a**) 3D schematic of the unit cell of the metamaterial on CaF_2 substrate. (**b**) SEM image of the sample.

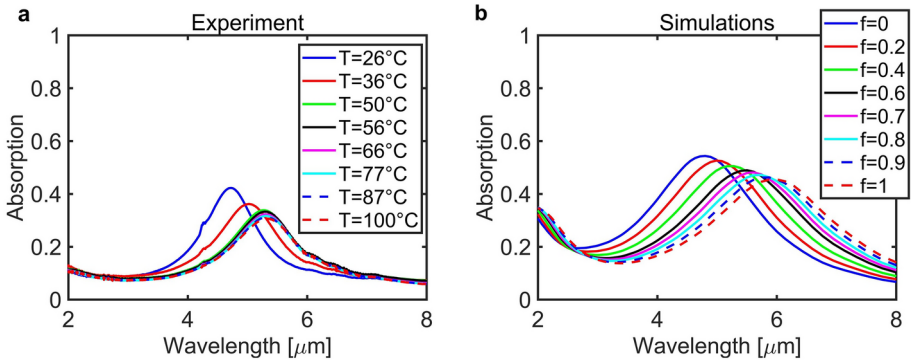

Fig. 2. (**a**) Experimental spectra showing the resonance tuning of the metamaterial with the temperature. (**b**) Simulation using Bruggeman formalism and Looyenga mixing rule; f is the fitting parameter which represents the fraction of metallic VO_2 during the heating.[40,41].

Experimental T [°C]	Resonant wavelength [μm]	Absorption	Absorption @4.72 μm
26	4.720	0.42	0.42
36	5.024	0.36	0.31
37	5.025	0.36	0.30
49	5.290	0.34	0.22
56	5.290	0.33	0.21
66	5.302	0.32	0.21
77	5.319	0.32	0.20
87	5.330	0.31	0.20
100	5.334	0.31	0.20

Table 1. Experimental values obtained for the resonant wavelengths and corresponding absorption values.

as a function of the temperature. The observed wavelength tuning range is continuous and broadband since the reflectance dip reaches 5.43 μm at 66 °C, spanning for more than 0.5 μm while the reflection dip becomes shallower. We also assessed the reversibility by cooling the sample down to room temperature and checked the reestablishment of the dip at 4.72 μm even after repeatedly heating/cooling cycles. Although stable and reproducible, the obtained experimental values differ from the designed (ideal) dynamic range (as studied in ref.[33]), which was expected to be higher (about 1) when the VO_2 switches to metallic state.

To shed light on such effects, we present the numerical fitting procedure which allows us to reconstruct the electromagnetic metamaterial behavior at the micro/nanoscale as the temperature changes. Starting from the fabricated geometric parameters, our goal was to match the simulated absorption spectra with the experimental data at both the highest and lowest temperatures, as well as in the intermediate states. We first used effective-medium approach combined with Bruggeman formalism to retrieve the refractive indices of VO_2 during the transition[9,42,43] by assuming that in the intermediate states both semiconductor and metallic domains coexist. The best fitting value for the starting (semiconductor-like) state of the VO_2 was found to be $n_{cold} = 2.7 + 0.6i$. Meanwhile, the optimal fit of the VO_2 state at the highest temperature (metal-like) was found to be $n_{hot} = 3.4 + 0.7i$. These parameters were then used as constant, while we introduced a volume filling factor f as the fraction of the metallic phase which increases with the temperature T: f changes the effective complex refractive index of VO_2 according to Looyenga mixing rule.[9,44] By using f as a fitting parameter, the resulting fitting process yielded theoretical curves that closely match the experimental results, as reported in Fig. 2b. However, we note the extracted complex refractive indices differ from the ones previously reported by both our[4] and other groups[9,25], suggesting a potentially incomplete SMT.

In Table 1, we further report the experimentally measured wavelengths of the absorption peaks and the corresponding absorption for different temperature values. In the last column, the absorption at a fixed wavelength, corresponding to the room temperature "semiconductor" absorption peak (@4.72 μm) is shown. We note that the fabrication parameters were obtained following an optimization process with initial refractive indices values reported in ref.[4]. Using such optimized parameters, we predicted a dynamic absorption range of 0.8 at around 4.3 μm. Moreover, in previous numerical investigation of such design, the dynamic absorption range was proven to be robust to variations of VO_2 thickness as high as 10%.[33] However, in the experiment, we observed that at room temperature, the peak is positioned at approximately 4.72 μm, and it results in significantly lower dynamic absorption range.

The main reasons for the observed discrepancies could be ascribed to the inhomogeneity, in terms of density and optical parameters (e.g., refractive index), of the very thin VO_2 film, which are different than those of thicker films having a different growth regime; such effects were recently experimentally demonstrated in ref.[37]. This

means that the optical parameters of the 60 nm-thick VO_2 film, extrapolated by our measurements, may be slightly different than those expected, which refer typically to fully formed VO2 films.

Our results provide a proof of concept of the wavelength and intensity tunability using a hybrid metamaterial based on VO_2 phase change. Strategies to overcome technological issues and obtain enhanced/optimized performances will be considered in further work.

In thermodynamic equilibrium, the tuning of the absorption corresponds to the tuneable emissivity. Therefore, in Fig. 3a, we focus on the absorption intensity tuning at the resonant wavelength of the semiconductor-like state (at 4.72 μm); the calculation details for absorption density ρ_{abs} and total absorption are given in *Methods*. When the fraction f of the metallic VO_2 phase is increased, the absorption peak gradually becomes lower, following an almost linear trend, as it can be seen on the left axis in Fig. 3a. A similar trend can be seen in experimentally extracted values of absorption at the same wavelength for the different temperatures, reported on the right y-axis of Fig. 3a. Blue, green and red stars on the graph represent the total simulated absorption when the fitting factor f is equal to 0 (semiconductor-like), 0.6 (intermediate) and 1 (metal-like).

In Fig. 3b, we further visualize 3D distribution of ρ_{abs} in the unit cell, calculated for f = 0, f = 0.6 and f = 1. The obtained results highlight that for f = 0 (i.e. semiconductor-like state), there is a strong absorption between the two metallic layers, due to the plasmonic gap resonances. The absorption decreases as f increases. When the filling factor reaches the unity value, at f = 1, we notice much lower absorption due to the red-shift of the resonant wavelength for the metal-like VO_2 state. In Fig. 3c, we highlight the plasmonic gap resonances generating an extremely strong magnetic field in the VO_2 layer. Furthermore, the magnetic resonance can be temperature-controlled since heating of the VO_2 leads to the increase in the reflectivity, and subsequently switches off the resonance. This feature can be harnessed for several magnetic-dipole based applications.[20,31,45]

Finally, we show the tuning of the absorption peak resonance as a function of both theoretically calculated filling factor, and the measured temperature. In Fig. 4a, simulated filling factor values (continuous line) show a linear behavior as a function of the fitting parameter f: the resonance is red-shifted with increasing metallic phase content. The blue and the red stars represent the simulated resonant wavelength for the fitting parameter f = 0 (semiconductor-like state) and f = 1 (metal-like state). On the other hand, the experimental values of resonant

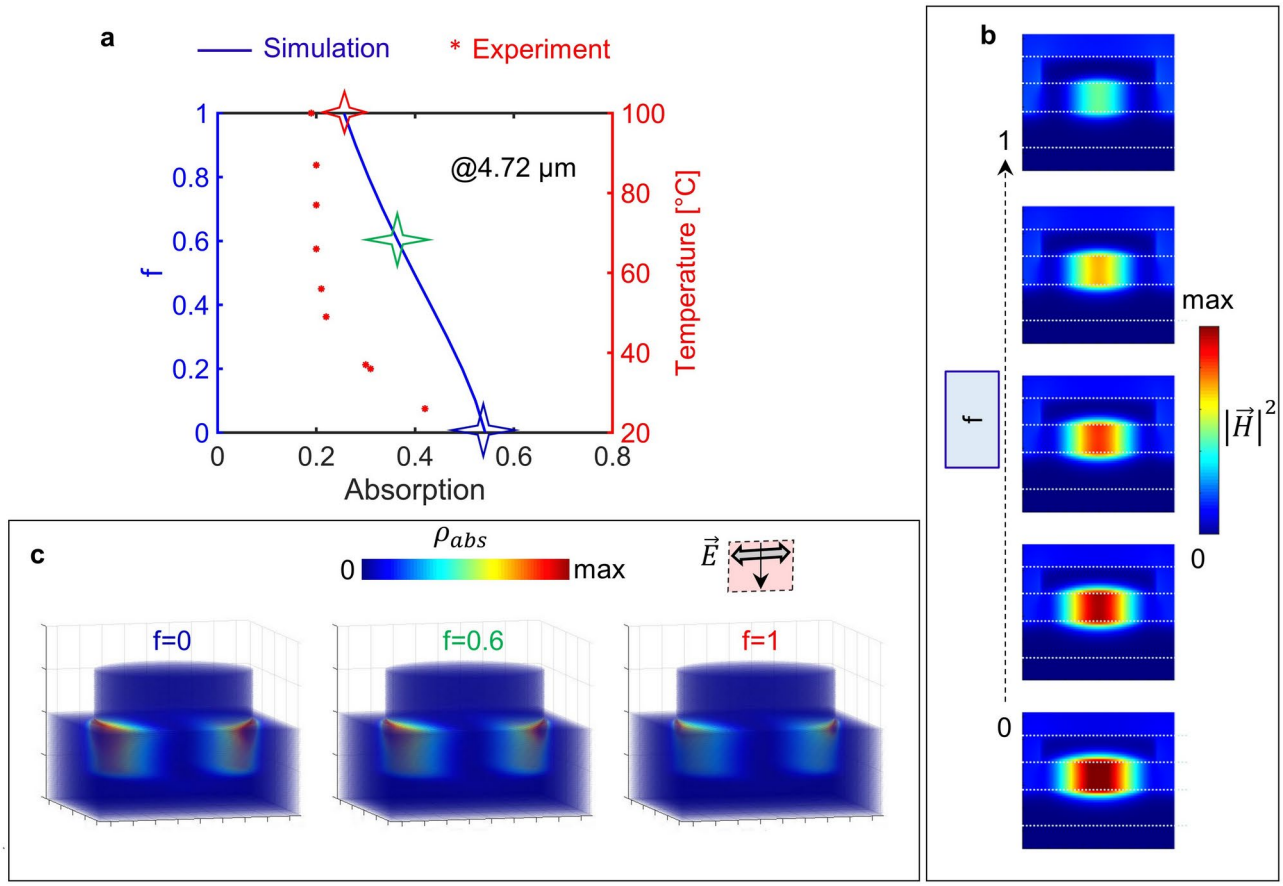

Fig. 3. (**a**) Simulated and experimental absorption intensity at the resonant wavelength for the purely semiconductor VO_2. Blue, green and red stars on the graph represent the total simulated absorption when the fitting parameter f is equal to 0 (semiconductor-like), 0.6 (intermediate) and 1 (metal-like). Heating increases reflection, hence decreasing absorption, as shown in (**b**): 3D distribution of the absorption density at f = 0, f = 0.6 and f = 1. (**c**) Magnetic field intensity as a function of the volume parameter f; the strong magnetic field at the resonant wavelength and f = 0, is gradually switched off as f increases.

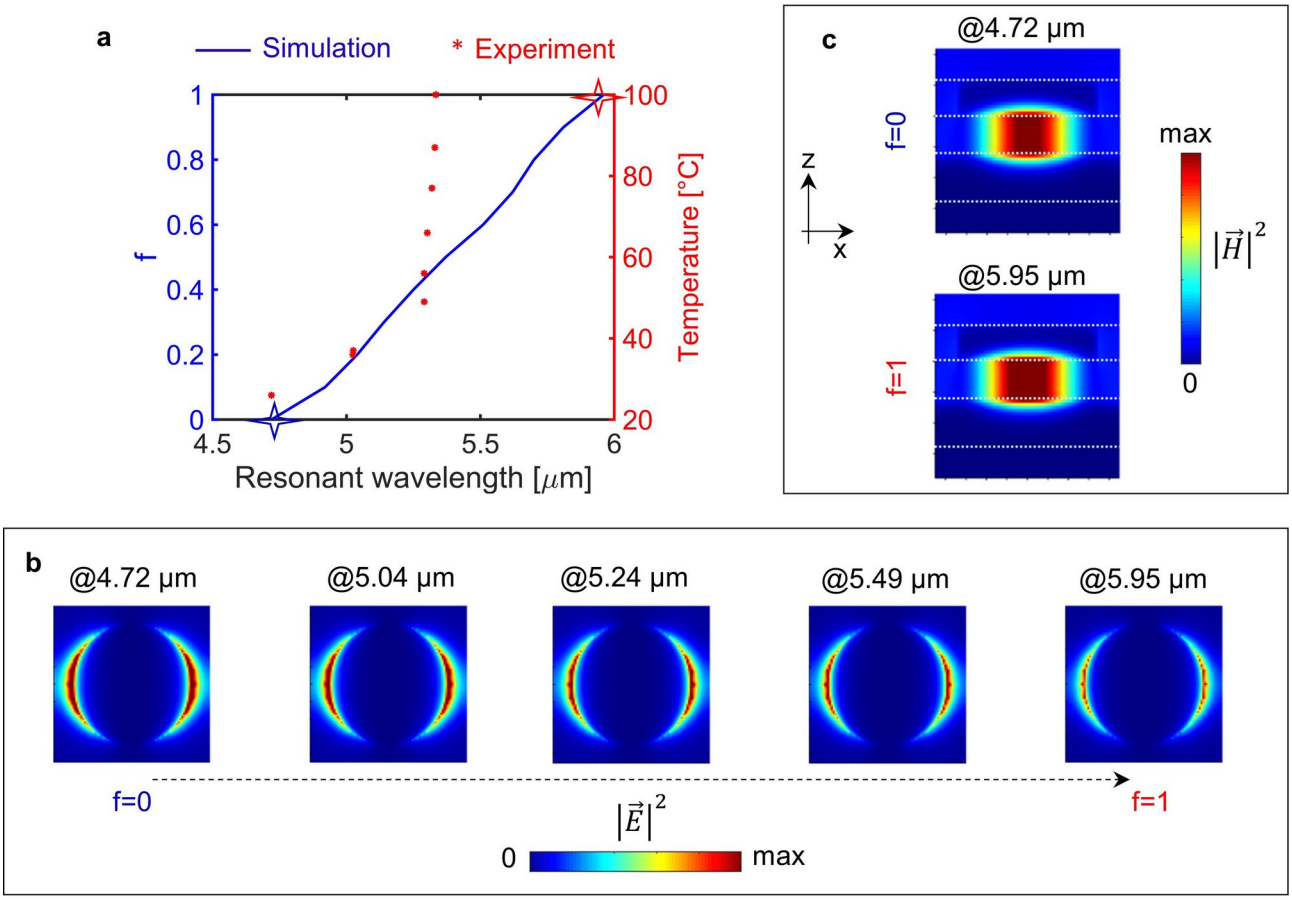

Fig. 4. (**a**) Simulated and experimental results for the resonant wavelength as a function of the fitting parameter f (simulation, left axis) and temperature (experiment, right axis), respectively. The blue and the red stars represent the simulated resonant wavelength for the fitting parameter f = 0 (semiconductor-like state) and f = 1 (metal-like state). (**b**) Distribution of the electric field in the xy-plane positioned 10 nm above the Au nanodisk: resonant wavelengths and the enhancement red-shift with the increase of the factor f. (**c**) xz-monitor of the simulated magnetic field intensity at resonant wavelengths for f = 0 (4.72 μm) and f = 1 (5.95 μm).

wavelengths are shown as a function of the temperature (right y-axis). While there is a good agreement for the resonant wavelength in the lower temperature range, there is a discrepancy for the behavior at temperatures above 60 °C since the resonant wavelength stabilizes around 5.43 μm. As already mentioned, we attribute these differences to the complex fabrication process leading to material modifications with respect to ideal VO_2. Another issue is the fact that we used two average refractive indices for the semiconducting and metallic VO_2 phases, i.e. for f = 0 and f = 1 respectively. In order to better match experimental results with the theoretical calculated values, one would need the ellipsometric characterization for VO_2 fabricated with the same procedure and under same conditions. Nevertheless, in the low-temperature range, this device can tune the absorption peak wavelength without drastically altering its absolute value (Table 1). Accordingly, the electromagnetic fields, as it can be appreciated in Fig. 4b, show similar distributions at increasing resonant wavelengths, i.e. when factor f increases. Finally, at resonant wavelengths for f = 0 (4.72 μm) and f = 1 (5.96 μm), the resonant magnetic field is largely concentrated in the VO_2 gap between the Au nanodisk and the Au ground layer, Fig. 4c.

Conclusion

In conclusion, we fabricated a VO2-based hybrid metamaterial and experimentally demonstrated the infrared tuning of the resulting gap plasmon resonance. Heating the metamaterial from 26 to 100 °C results into the reversible resonance shift from 4.72 to 5.34 μm. Finally, we have employed numerical modelling to retrieve the effective refractive indices of the VO2 binary system, composed by semiconductor and metallic phases, during the heating process. Numerical calculations highlight that strongly confined magnetic field at the resonant wavelength can be tuned in both intensity and wavelength by temperature control. Even though the total semiconductor-to-metal phase transition was not achieved, the observed tuning is found to be reconfigurable and highly repeatable. We are confident that the investigated design can be refined and improved for optimal tunable absorber applications in the infrared, paving the way for applications where strong absorption contrast over a broad wavelength range is required.

Methods

Numerical simulations

FDTD domain surrounds the MIM structure with Bloch boundary conditions (BBCs) in the xy-plane, and the Perfectly Matched Layers (PMLs) in the z-direction. We performed convergence testing to ensure simulation stability in terms of PML properties and distance from the structure (at least one maximum wavelength). The structure is then excited by a linearly polarized plane-wave in the 2–8 μm range coming from the air side. The absorption density in each point of the unit cell is calculated from 3D electric field $\boldsymbol{E}$ and complex permittivity ε monitors at frequency ω as: $\rho_{abs} = -0.5 \cdot \omega \cdot \left| \boldsymbol{E}^2 \right| \cdot \mathrm{imag}(\varepsilon)$; the total absorption is then calculated integrating ρ_{abs} over the unit cell volume. The refractive indices of CaF_2 substrate and Au are taken from the Lumerical database, while the initial (pre-fabrication) modelling of VO_2 was based on our experimental results from ref.[4]. Specifically, the best fitting parameters in that study provided average refractive indices for the MWIR for metallic and semiconductor phases of VO_2. The optimization was performed by switching the material properties of VO_2 layer from semiconductor to metallic and then monitoring the resulting optimal contrast between the two states. The optimization procedure leads to the resulting optimal nanodisk parameters of h = 60 nm, r = 345 nm, and periodicity p = 900 nm, while the optimized thicknesses for VO_2 and Au background layers was calculated to be 60 nm and 80 nm, respectively.

Fabrication of the VO_2-hybridized metasurface

The device was realized starting from a 1 mm-thick CaF_2 substrate. It underwent a cleaning process using an ultrasonic bath containing acetone, isopropyl alcohol (IPA), and distilled water (2 min for each step). Harsh impurities were removed by using oxygen plasma cleaning for 3 min. Subsequently, an 80 nm thick gold layer was grown on the sample using electron beam physical vapor deposition (e-beam PVD), followed by a 60 nm-thick VO_2 layer obtained by PLD. On top of the VO_2 film, a poly(methylmethacrylate) (PMMA) electron-sensitive resist was spin-coated at 1800 rpm for 1 min and dried on a hotplate at 180 °C for 7 min. The PMMA was then patterned by electron beam lithography at 20 kV with a dose of 500 μC/cm^2 and developed in a solution of Methyl isobutyl ketone (MIBK) and IPA (1:3 in volume) at 4 °C for 30 s, stopped in IPA for 30 s and dried with a nitrogen flow. The sample was finally covered with 60 nm of Au by e-beam PVD, and then immersed in hot acetone to remove via lift-off the unexposed resist.

Data availability

The datasets used and/or analysed during the current study available from the corresponding author on reasonable request.

Received: 19 July 2024; Accepted: 3 October 2024
Published online: 25 October 2024

References

1. Qazilbash, M. M. et al. Mott transition in VO_2 revealed by infrared spectroscopy and nano-imaging. *Science***318**(5857), 1750–1753 (2007).
2. Wu, C., Feng, F. & Xie, Y. Design of vanadium oxide structures with controllable electrical properties for energy applications. *Chem. Soc. Rev.***42**, 5157 (2013).
3. Liu, K. et al. Recent progresses on physics and applications of vanadium dioxide. *Mater. Today***21**, 875 (2018).
4. Cesca, T. et al. Correlation between in situ structural and optical characterization of the semiconductor-to-metal phase transition of VO_2 thin films on sapphire. *Nanoscale***12**, 851 (2020).
5. Larciprete, M. C. et al. Tunable IR perfect absorbers enabled by tungsten doped VO_2 thin films. *APL Materials***11**, 091107 (2023).
6. Bile, A. et al. Room-temperature tuning of mid-infrared optical phonons and plasmons in W-doped VO_2 thin films. *Opt. Mater.***154**, 115732 (2024).
7. Kakiuchida, H., Jin, P., Nakao, S. & Tazawa, M. T. Optical properties of vanadium dioxide film during semiconductive-metallic phase transition. *Jpn. J. Appl. Phys.***46**, 113 (2007).
8. Kats, A. et al. Vanadium dioxide as a natural disordered metamaterial: Perfect thermal emission and large broadband negative differential thermal emittance. *Phys. Rev. X***3**, 041004 (2013).
9. Wan, C. et al. On the optical properties of thin-film vanadium dioxide from the visible to the far infrared. *Ann. Phys.***531**, 1900188 (2019).
10. Taha, M. et al. Insulator–metal transition in substrate-independent VO_2 thin film for phase-change devices. *Sci. Rep.***7**, 17899 (2017).
11. Golubev, V. G. et al. Phase transition-governed opal–VO_2 photonic crystal. *Appl. Phys. Lett.***79**, 2127–2129 (2001).
12. Barimah, E. K. et al. Infrared optical properties modulation of VO_2 thin film fabricated by ultrafast pulsed laser deposition for thermochromic smart window applications. *Sci. Rep.***12**, 11421 (2022).
13. Kim, H. et al. VO_2-based switchable radiator for spacecraft thermal control. *Sci. Rep.***9**, 11329 (2019).
14. Larciprete, M. C. et al. Effect of heating/cooling dynamics in the hysteresis loop and tunable IR emissivity of VO_2 thin films. *Opt. Exp.***28**, 39203 (2020).
15. Larciprete, M. C. et al. Adaptive tuning of infrared emission using VO_2 thin films. *Sci. Rep.***10**, 11544 (2020).
16. Abedini Dereshgi, S. et al. Tuning of optical phonons in α-MoO_3-VO_2 multilayers. *ACS Appl. Mater. Interfaces***13**, 48981 (2021).
17. Azad, S. et al. VO_2 thin film enabled free space modulation of infrared light using pulsed electric field. *ACS Photonics***11**, 2138–2149 (2024).
18. Bohaichuk, S. M. et al. Localized triggering of the insulator-metal transition in VO_2 using a single carbon nanotube. *ACS Nano***13**, 11070–11077 (2019).
19. Pevtsov, A. B. et al. Ultrafast stop band kinetics in a three-dimensional opal-VO_2 photonic crystal controlled by a photoinduced semiconductor-metal phase transition. *Phys. Rev. B***75**, 153101 (2007).
20. Appavoo, K. et al. Ultrafast phase transition via catastrophic phonon collapse driven by plasmonic hot-electron injection. *Nano Lett.***14**, 1127–1133 (2014).
21. Cueff, S. et al. Dynamic control of light emission faster than the lifetime limit using VO_2 phase-change. *Nat. Commun.***6**, 8636 (2015).
22. Kats, M. A. et al. Ultra-thin perfect absorber employing a tunable phase change material. *Appl. Phys. Lett.***101**, 221101 (2012).

23. Pradhan, J. K. et al. High contrast switchability of VO_2 based metamaterial absorbers with ITO ground plane. *Opt. Express***25**(8), 9116–9121 (2017).
24. Driscoll, T. et al. Dynamic tuning of an infrared hybrid-metamaterial resonance using vanadium dioxide. *Appl. Phys. Lett.***93**, 024101 (2008).
25. Dicken, M. J. et al. Frequency tunable near-infrared metamaterials based on VO_2 phase transition. *Opt. Express***17**, 18330 (2009).
26. Kocer, H. et al. Thermal tuning of infrared resonant absorbers based on hybrid gold-VO_2 nanostructures. *Appl. Phys. Lett.***106**, 161104 (2015).
27. Yang, L. et al. Broadband thermal tunable infrared absorber based on the coupling between standing wave and magnetic resonance. *Opt. Mater. Express***7**, 2767–2776 (2017).
28. Boyce, A. M. et al. Actively tunable metasurfaces via plasmonic nanogap cavities with sub-10-nm VO_2 films. *Nano Lett.***22**, 3525 (2022).
29. Sun, K. et al. VO_2 thermochromic metamaterial-based smart optical solar reflector. *ACS Photonics***5**, 2280–2286 (2018).
30. Sun, K. et al. VO_2 metasurface smart thermal emitter with high visual transparency for passive radiative cooling regulation in space and terrestrial applications. *Nanophotonics***11**(17), 4101–4114 (2022).
31. Osgouei, A. K. et al. Active tuning from narrowband to broadband absorbers using a sub-wavelength VO_2 embedded layer. *Plasmonics***16**, 1013–1021 (2021).
32. Petronijevic, E. et al. Control of Au nanoantenna emission enhancement of magnetic dipolar emitters by means of VO_2 phase change layers. *Opt. Express***27**, 24260 (2019).
33. Petronijevic, E. & Sibilia, C. Thin films of phase change materials for light control of metamaterials in the optical and infrared spectral domain. *Opt. Quantum Electron.***52**, 110 (2020).
34. Xiao, L. et al. Fast adaptive thermal camouflage based on flexible VO_2/Graphene/CNT thin films. *Nano Lett.***15**, 8365–8370 (2015).
35. Long, L., Taylor, S., Ying, X. & Wang, L. Thermally-switchable spectrally-selective infrared metamaterial absorber/emitter by tuning magnetic polariton with a phase-change VO_2 layer. *Mater. Today Energy***13**, 214e220 (2019).
36. Conde Garrido, J. M. & Silveyra, J. M. A review of typical PLD arrangements: Challenges, awareness, and Solutions. *Opt. Lasers Eng.***168**, 107677 (2023).
37. Li Voti, R. et al. Optothermal characterization of vanadium dioxide films by infrared thermography. *Int. J. Therm. Sci.***197**, 108832 (2024).
38. Carrara, A. et al. Plasmon hybridization in compressible metal–insulator–metal nanocavities: An optical approach for sensing deep sub-wavelength deformation. *Adv. Opt. Mater.***8**, 2000609 (2020).
39. Petronijevic, E. et al. Extrinsic chirality and circular dichroism at visible frequencies enabled by birefringent α-MoO_3 nanoscale-thick films: Implications for chiro-optical control. *ACS Appl. Nano Mater.***5**, 5609 (2022).
40. Lumerical Solutions, Inc. http://www.lumerical.com/tcadproducts/fdtd/
41. Petronijevic, E. et al. Near-infrared modulation by means of GeTe/SOI-based metamaterial. *Opt. Lett.***44**, 1508 (2019).
42. Rensberg, J. et al. Active optical metasurfaces based on defect-engineered phase-transition materials. *Nano Lett.***16**(2), 1050–1055 (2016).
43. Cesarini, G. et al. Quantitative evaluation of emission properties and thermal hysteresis in the mid-infrared for a single thin film of vanadium dioxide on a silicon substrate. *Int. J. Therm. Sci.***146**, 106061 (2019).
44. Tognazzi, A. et al. Opto-thermal dynamics of thin-film optical limiters based on the VO_2 phase transition. *Opt. Mater. Express***13**(1), 41–52 (2023).
45. Kalinic, B. et al. Active modulation of Er^{3+} emission lifetime by VO_2 phase-change thin films. *Adv. Photonics Res.***5**, 2300242 (2024).

Acknowledgements

The authors would like to thank Mariangela Cestelli Guidi at INFN-LNF Dafne-Light for her hospitality and support with experiments using FTIR microscopy and acknowledge the experimental support of Giancarlo della Ventura at Dipartimento di Scienze (Università Roma Tre) and INFN-LNF. M.C.L. and R.M. acknowledge partial support from the European Union- NextGenerationEU (Bando PRIN 2022, Directorial Decree n. 104 February 02, 2022, CUP B53D23009050006 Project code: 2022ZRN4LX PNRR M4.C2.1.1). The opinions expressed are those of the authors only and should not be considered representative of the European Union or the European Commission's official position. Neither the European Union nor the European Commission can be held responsible for them.

Author contributions

E.P., C.S. and R.L.V. conceptualized the study. V.A., L. R., A. T. and R. M. fabricated the samples. M. C. L., M. C. and L. P. performed the experiments, collected and analyzed data. E. P. drafted the manuscript, which was critically revised by R.M, M.C.L. and M. C. All authors read and agreed to submit the final manuscript.

Competing interests

The authors declare no competing interests.

Additional information

Correspondence and requests for materials should be addressed to M.C.L.

Reprints and permissions information is available at www.nature.com/reprints.

Publisher's note Springer Nature remains neutral with regard to jurisdictional claims in published maps and institutional affiliations.